AIP | Applied Physics Letters

Visualization of dielectric constant-electric field-temperature phase maps for imprinted relaxor ferroelectric thin films

J. C. Frederick, T. H. Kim, W. Maeng, A. A. Brewer, J. P. Podkaminer, W. Saenrang, V. Vaithyanathan, F. Li, L.-Q. Chen, D. G. Schlom, S. Trolier-McKinstry, M. S. Rzchowski, and C. B. Eom

Citation: Applied Physics Letters **108**, 132902 (2016); doi: 10.1063/1.4944774
View online: http://dx.doi.org/10.1063/1.4944774
View Table of Contents: http://scitation.aip.org/content/aip/journal/apl/108/13?ver=pdfcov
Published by the AIP Publishing

Visualization of dielectric constant-electric field-temperature phase maps for imprinted relaxor ferroelectric thin films

J. C. Frederick,[1] T. H. Kim,[1] W. Maeng,[1] A. A. Brewer,[1] J. P. Podkaminer,[1] W. Saenrang,[1] V. Vaithyanathan,[2] F. Li,[3] L.-Q. Chen,[3] D. G. Schlom,[2] S. Trolier-McKinstry,[3] M. S. Rzchowski,[4] and C. B. Eom[1,4,a)]

[1]*Department of Materials Science and Engineering, University of Wisconsin-Madison, Madison, Wisconsin 53706, USA*
[2]*Department of Materials Science and Engineering, Cornell University, Ithaca, New York 14853, USA*
[3]*Department of Materials Science and Engineering, Pennsylvania State University, University Park, Pennsylvania 16802, USA*
[4]*Department of Physics, University of Wisconsin-Madison, Madison, Wisconsin 53706, USA*

(Received 27 November 2015; accepted 3 March 2016; published online 28 March 2016)

The dielectric phase transition behavior of imprinted lead magnesium niobate–lead titanate relaxor ferroelectric thin films was mapped as a function of temperature and dc bias. To compensate for the presence of internal fields, an external electric bias was applied while measuring dielectric responses. The constructed three-dimensional dielectric maps provide insight into the dielectric behaviors of relaxor ferroelectric films as well as the temperature stability of the imprint. The transition temperature and diffuseness of the dielectric response correlate with crystallographic disorder resulting from strain and defects in the films grown on strontium titanate and silicon substrates; the latter was shown to induce a greater degree of disorder in the film as well as a dielectric response lower in magnitude and more diffuse in nature over the same temperature region. Strong and stable imprint was exhibited in both films and can be utilized to enhance the operational stability of piezoelectric devices through domain self-poling. © *2016 AIP Publishing LLC*.
[http://dx.doi.org/10.1063/1.4944774]

Understanding the dielectric behaviors in relaxor ferroelectrics (FEs) is of great importance not only for studying thermally induced phase transitions, but also for high performance electromechanical actuators and sensors.[1,2] Relaxor FEs, in contrast to conventional FEs, are characterized by suppression of long-range ordering of the spontaneous polarization and derive their dielectric behaviors from localized polar nano-regions. The polar nano-regions persist above a temperature T_{max}, at which the relative dielectric constant (ε_r) is maximum, whereas they become frozen into a disordered glassy state at temperatures below T_{max}.[3] Especially, in the vicinity of the morphotropic phase boundary, where relaxor-based FEs undergo a structural transition induced by changes in chemical composition, large dielectric responses and exceptional electromechanical properties have been observed.[4] For solid-solutions of the prototypical relaxor FE $Pb(Mg_{1/3}Nb_{2/3})O_3$ with the normal FE $PbTiO_3$ (PMN-PT), ultrahigh piezoelectric coefficient of 2000–3000 pC/N is reported.[5] Recently, high-performance piezoelectric MEMS (micro-electromechanical systems) devices have been demonstrated by exploiting PMN-PT thin films on $SrTiO_3$ (STO)-buffered Si substrates, exhibiting strong piezoelectricity and a good figure of merit $(e_{31,f}^2/\varepsilon_r\varepsilon_0)$ for energy harvesting applications.[6] In particular, the enhanced figure of merit was aided by a large imprint of ~ -40 kV/cm, which suppressed ε_r at the zero-field condition; tuning the system to exhibit stronger imprint may further suppress ε_r, in turn augmenting the energy harvesting performance of such films operating in the e_{31} mode.

Imprint strongly affects the dielectric behaviors of relaxor-based FE thin films. Imprint, which manifests as a lateral shift in polarization (P)-electric field (E) hysteresis loops, originates from the presence of internal electric fields.[7] Given that the relative dielectric permittivity, ε_r, is proportional to dP/dE,[8] the dielectric behaviors in imprinted relaxor FE thin films are also shifted along the E-axis in accordance with the magnitude and direction of the internal electric fields. In order to understand the dielectric behaviors in specimens with imprinted hysteresis, an external E bias with the same magnitude and the opposite direction should be applied to compensate internal fields while measuring the T-dependence of the dielectric responses.[9] Because this is rarely done, the influence of the imprint on the dielectric properties and its temperature-dependent stability is not well studied.[10–15]

In this work, three-dimensional (3D) dielectric maps were visualized in order to investigate the imprint effect on the dielectric response of relaxor FE PMN-PT thin films. This was accomplished by repeatedly measuring ε_r–E loops with increasing T and then constructing 3D ε_r–E-T phase maps by integrating the measured dielectric hysteresis loops with respect to T. Based on the constructed dielectric maps, the relationship between structural and dielectric properties in the PMN-PT thin films is discussed in conjunction with disorder inside the films.

For this aim, two epitaxial 0.70PMN-0.30PT thin films with different strain states were prepared using rf magnetron sputtering. Through a comparison with bulk PMN-PT, it was

a)Author to whom correspondence should be addressed. Electronic mail: ceom@wisc.edu

found that a Pt (40 nm)/PMN-PT (500 nm)/$SrRuO_3$ (100 nm) film on a STO (001) substrate is under in-plane compressive strain [Fig. 1(a)], whereas another Pt (40 nm)/PMN-PT (500 nm)/$SrRuO_3$ (100 nm) film on a STO-buffered Si substrate is under in-plane tensile strain [Fig. 1(b)]. Detailed information on the in-plane and out-of-plane lattice constants is given in supplementary Table S1.[16] The in-plane and out-of-plane lattice parameters were obtained by measuring *d*-spacings of {103} and (002) Bragg peaks at a bisecting condition of the X-ray scattering vector of PMN-PT films. It should be noted that the film on STO-buffered Si exhibited a change in unit cell volume (+1.3%) that cannot be explained solely by elastic deformation, suggesting incorporation of defects into the lattice. Defect-mediated strain accommodation (e.g., via oxygen vacancy formation) resulting in chemical expansion of the unit cell has been reported elsewhere in similar complex-oxide thin films.[17,18]

STO and Si substrates with 4° miscut toward [110] were used to reduce domain variants due to rhombohedral symmetry of bulk 0.7PMN-0.3PT.[19] For both PMN-PT thin films, no impurity phase was detected in a wide range of θ–2θ scans [Figs. 1(c) and 1(d)]. In-plane epitaxy was confirmed via ϕ scans [supplementary Figs. S1(a) and S1(b)], and along with the out-of-plane θ–rocking curves [supplementary Figs. S1(c) and S1(d)] indicating high crystalline quality.[16] Electrical measurements were performed in Pt/PMN-PT/$SrRuO_3$ capacitors 100 μm in diameter. *P-E* hysteresis loops were collected by applying triangular pulse fields with the amplitude of 240 kV/cm at a frequency of 1 kHz using a Precision Multiferroic tester (Radiant Technologies, Inc.). Dielectric constant and loss data were recorded under ac fields with the amplitude of 50 mV and the frequency of 100 kHz using a precision LCR meter (Hewlett Packard 4284A).

Figures 2(a) and 2(b) show *P-E* and ε_r–*E* hysteresis loops of PMN-PT thin films on STO and STO-buffered Si (001) substrates at room temperature, respectively. A larger remanent polarization (P_r) of ~27.3 $\mu C/cm^2$ was observed in the PMN-PT films on STO (001) substrates than that of ~9.7 $\mu C/cm^2$ in PMN-PT films on STO-buffered Si (001) substrates. Considering that the films on STO and STO-buffered Si substrates are under in-plane compressive and tensile strain with respect to bulk PMN-PT ($P_{r,bulk} \sim 30\ \mu C/cm^2$) (not shown here), respectively, the difference in P_r between the PMN-PT films is attributed to a strain effect.[20] In contrast, in dielectric hysteresis loops, the maximum dielectric constant ($\varepsilon_{r,max} \sim 1380$) in the PMN-PT films on STO (001) substrates is smaller than that (~1750) in the films on STO-buffered Si (001) substrates, although the effective tunability, $(\varepsilon_{r,max} - \varepsilon_{r,min})/\varepsilon_{r,max}$, is comparable between the two films. Interestingly, for the PMN-PT films on STO-buffered Si (001) substrates, a strong imprint of ~−65 kV/cm is observed in both *P-E* and ε_r–*E* hysteresis loops. Note that imprint in the PMN-PT films on STO (001) substrates is ~−15 kV/cm. Furthermore, the *T* dependence of the imprint is quite different for the PMN-PT films on STO and STO-buffered Si (001) substrates [Figs. 2(c) and 2(d)]. For the PMN-PT films on STO substrates, the absolute value of the imprint decreases with increasing *T*, whereas it is almost constant in the films on STO-buffered Si substrates. This *T* dependence of the imprint emphasizes the necessity of *E* sweep in *T*-dependent dielectric response measurements in relaxor FE thin films.

3D maps of ε_r, *E*, and *T* in PMN-PT thin films are shown in Fig. 3. To achieve this, ε_r–*T* loops were obtained by sweeping electric fields from negative to positive bias in a stepwise manner at room temperature as shown Fig. 2(b);

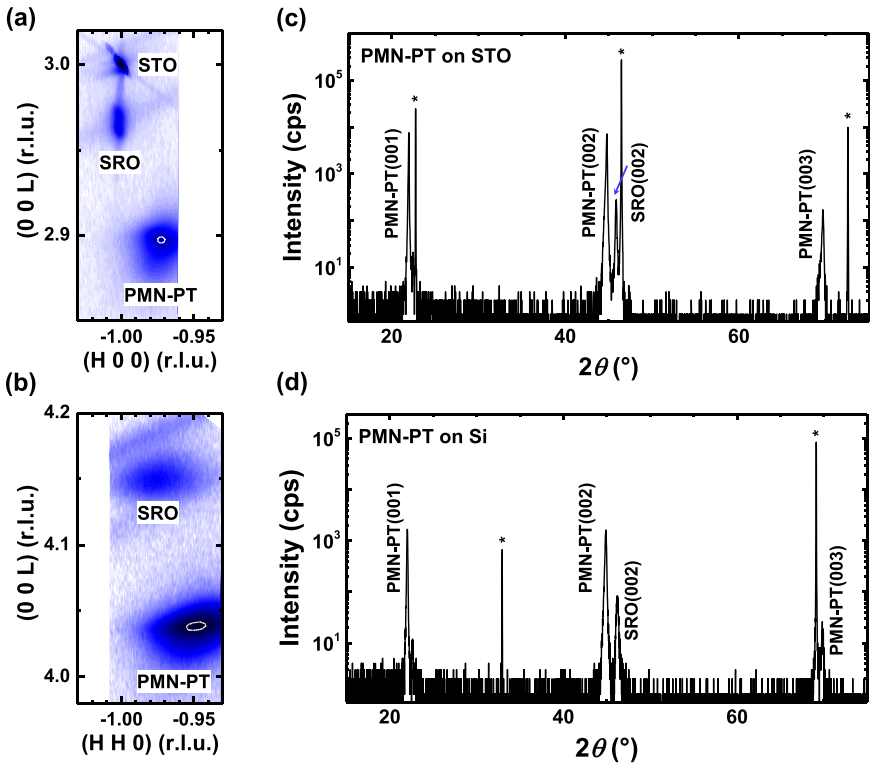

FIG. 1. Structural characterization of 500-nm-thick epitaxial 0.7PMN-0.3PT films. Reciprocal space maps show the in-plane strain states of 0.7PMN-0.3PT films on (a) STO and (b) STO-buffered Si (001) substrates. Both films exhibit phase purity and in-plane epitaxy as indicated by X-ray diffraction. 2θ-θ scans, as shown for the film on (c) STO and (d) STO-buffered Si (001) substrates, respectively.

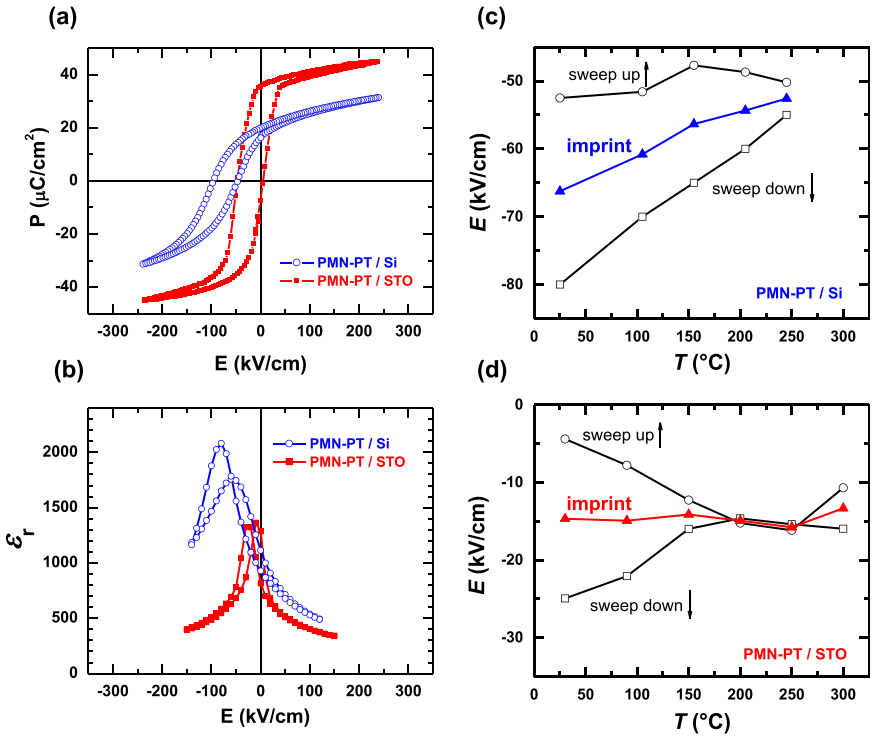

FIG. 2. Room temperature: (a) polarization (P)–electric field (E) and (b) dielectric constant (ε_r)–electric field (E) hysteresis loops for 0.7PMN-0.3PT films on STO (solid red squares) and STO-buffered Si (open blue circles) substrates. The change in the imprint (taken as the average of E_{max} during sweep up and sweep down) as a function of temperature (T) for the film on Si and STO-buffered STO is observed in (c) and (d), respectively, based upon the dc bias sweep during which the dielectric properties were measured.

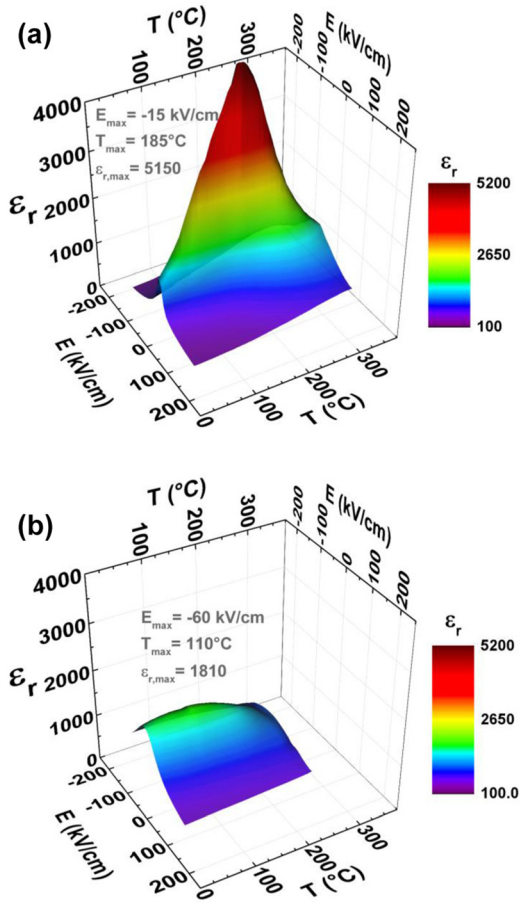

FIG. 3. Three-dimensional relative dielectric constant (ε_r)–external electric field (E)–temperature (T) maps of 0.7PMN-0.3PT films on (a) STO and (b) STO-buffered Si (001) substrates. Measurements were performed with a 100 kHz ac signal and from negative to positive dc bias during heating.

this procedure was repeated at discrete T intervals of 10 °C to yield comprehensive 3D dielectric maps. For more details of this measurement technique, see supplementary Fig. S2.[16] It was found that the true maximum values ($\varepsilon_{r,max}$, E_{max}, and T_{max}) in ε_r–E-T phase maps deviated from those at zero-field due to imprint. For the PMN-PT films on STO and STO-buffered Si substrates, $\varepsilon_{r,max}$ are 5150 and 1810, E_{max} are −15 and −60 kV/cm, and T_{max} are 185 and 110 °C, respectively.

Figs. 4(a) and 4(b) show that the dielectric behaviors in the PMN-PT films on STO-buffered Si substrates are more diffuse in both E- and T-axes than those on STO substrates. Figures 4(c) and 4(d) represent cross-sectional T-dependent dielectric responses on the planes of $E = E_{max}$ and $E = 0$. For both PMN-PT samples, it is clearly shown that dielectric responses at the electrically loaded condition are much larger than those at the zero-field condition in a wide range of T.

To examine the strain effect on dielectric phase transition in PMN-PT thin films, the dielectric behaviors of thin film samples were compared with that of bulk PMN-PT. This was done for the conditions where the internal fields in the thin films are compensated to facilitate comparison to the zero field data for bulk PMN-PT. As shown in Fig. 5(a), the dielectric permittivity in PMN-PT thin films is one order of magnitude smaller than the bulk value, consistent with a substrate clamping effect.[21] A shift in T_{max} is also observed in the two PMN-PT film samples; the PMN-PT films on STO-buffered Si substrates exhibit a maximum in ε_r at a slightly lower T ($\Delta T_{max} \sim -20$ °C), whereas the shift is towards higher T for the films on STO substrates ($\Delta T_{max} \sim 55$ °C). Such changes in T_{max} by substrate-induced strain are consistent with previous reports for epitaxial PMN-based films.[22] The T-dependent dielectric loss [Fig. 5(b)] also had a shifted T_{max}, almost identical to that in T-dependent dielectric permittivity data.

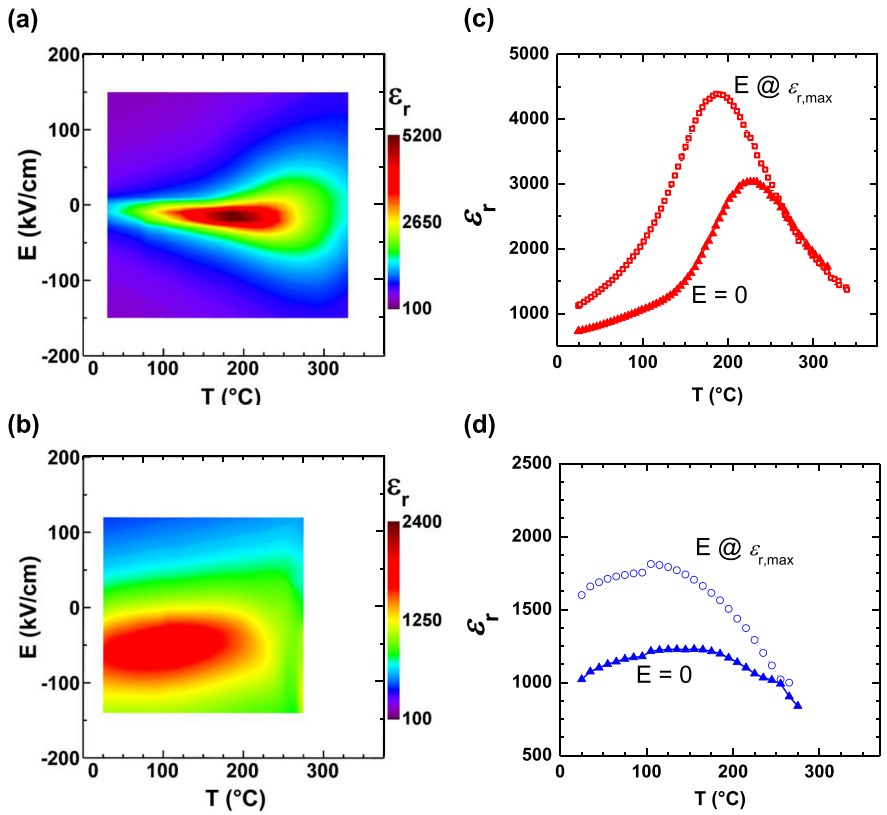

FIG. 4. Contour plots of the three-dimensional maps shown in Fig. 3 for 0.7PMN-0.3PT films on (a) STO and (b) STO-buffered Si (001) substrates. For emphasis, two-dimensional slices at a fixed E as indicated by the overlay show the T-dependent dielectric response of the films on (c) STO and (d) STO-buffered Si (001) substrates at the bias condition when ε_r is maximum (open symbols) and when the electric field is unloaded (solid symbols). Note the difference in scale between (a), (c) and (b), (d).

Dielectric peak broadening, indicative of a "smearing" out of the dielectric phase transition, was observed in both PMN-PT thin films, though it is more pronounced in the films on STO-buffered Si substrates. While the presence of an effective "dead" layer at the surface of a dielectric film has been demonstrated to suppress and broaden the dielectric response near T_C,[23,24] these results may also be a consequence, at least in part, of the epitaxial quality of the PMN-PT thin films. Note that incorporation of defects during growth can result in inhomogeneous strain fields within the film, broadening the phase transition.[25] Structural data (full-width half-maximum (FWHM) in rocking curve measurements and unit cell volume in the supplementary Table S1)[16] demonstrate that the film quality is inferior to that of the PMN-PT films on STO substrates, probably due to the existence of oxygen vacancy defects. The formation energy of oxygen vacancies in complex oxide films is reduced by tensile strain, supporting this conclusion.[26]

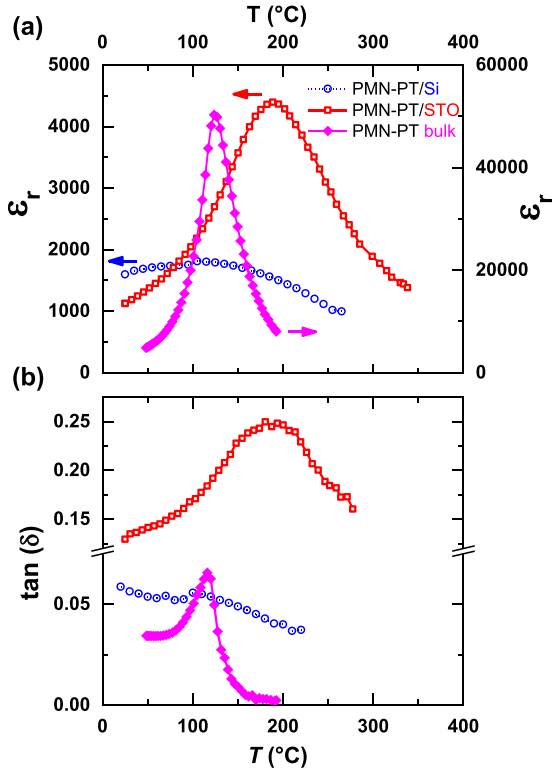

FIG. 5. T-dependent comparison of (a) dielectric constant and (b) loss tangent of 0.7PMN-0.3PT films on STO-buffered Si (a dashed line, open circles), STO (a solid line, open squares), and bulk single crystal 0.7PMN-0.3PT (a solid line, solid diamonds) at the E condition necessary to maximize ε_r. In the case of bulk, this is without any applied field.

It is important to consider the origin of the internal fields in PMN-PT thin films. In normal and relaxor FEs, various mechanisms for the internal field development have been proposed, including the existence of charged defects (trapped charges, defect dipole complexes), film/electrode interface effects (charge injection, the formation of passive or "dead" layers), the generation of built-in potential owing to asymmetric top and bottom electrodes, composition gradients, and flexoelectric fields induced by strain gradients.[27–29] Note that both PMN-PT thin films in this work have the same Pt top and $SrRuO_3$ bottom electrodes, suggesting that this alone cannot explain the large discrepancy in the magnitude of the imprint exhibited between the films on STO and STO-buffered Si substrates. Furthermore, the flexoelectric coefficient of PMN-PT would be insufficiently large to produce internal fields of the magnitude observed.[30] Considering that the strain states in two PMN-PT samples are relaxed throughout the film thickness, any flexoelectric field would

be negligible. Thus, considering that the PMN-PT thin films on STO-buffered Si substrates incorporate a number of vacancy defects, the internal fields may be attributed to composition gradients, charge trapping, or defect dipoles.

In summary, 3D ε_r–E–T phase maps of relaxor FE films with internal field bias were constructed. It was revealed that the shape and position of a ε_r peak in dielectric behaviors of PMN-PT thin films are quite different from the bulk properties depending on the strain state. Consequently, the construction of such 3D dielectric phase maps is crucial to visualizing the dielectric responses, as they can be strongly modified by internal fields. Furthermore, the internal bias field developed in the relaxor FE films is comparatively stable as a function of T. For applications to piezoelectric thin-film devices, the robust internal fields are of practical interest, leading to enhanced domain stability over a wide T range.[31]

This work was supported by the Army Research Office under Grant No. W911NF-13-1-0486. Li and Chen acknowledge the support from the National Science Foundation under Grant No. DMR-1410714.

[1]S. E. Park and W. Hackenberger, Curr. Opin. Solid State Mater. Sci. **6**, 11 (2002).
[2]S. Zhang and F. Li, J. Appl. Phys. **111**, 031301 (2012).
[3]X. J. Meng, D. Rémiens, M. Detalle, B. Dkhil, J. L. Sun, and J. H. Chu, Appl. Phys. Lett. **90**, 132904 (2007).
[4]Z. G. Ye, MRS Bull. **34**, 277 (2009).
[5]E. Sun and W. Cao, Prog. Mater. Sci. **65**, 124 (2014).
[6]S. H. Baek, J. Park, D. M. Kim, V. A. Aksyuk, R. R. Das, S. D. Bu, D. A. Felker, J. Lettieri, V. Vaithyanathan, S. S. N. Bharadwaja, N. Bassiri-Gharb, Y. B. Chen, H. P. Sun, C. M. Folkman, H. W. Jang, D. J. Kreft, S. K. Streiffer, R. Ramesh, X. Q. Pan, S. Trolier-McKinstry, D. G. Schlom, M. S. Rzchowski, R. H. Blick, and C. B. Eom, Science **334**, 958 (2011).
[7]S. Miller, J. Schwank, R. Nasby, and M. Rodgers, J. Appl. Phys. **70**, 2849 (1991).
[8]D. Damjanovic, Rep. Prog. Phys. **61**, 1267 (1998).
[9]N. Bassiri-Gharb, I. Fujii, E. Hong, S. Trolier-McKinstry, D. V. Taylor, and D. Damjanovic, J. Electroceram. **19**, 49 (2007).
[10]N. J. Donnelly, G. Catalan, C. Morros, R. M. Bowman, and J. M. Gregg, J. Appl. Phys. **93**, 9924 (2003).
[11]A. Laha and S. B. Krupanidhi, Mater. Sci. Eng., B **113**, 190 (2004).
[12]K. Wasa, I. Kanno, S. H. Seo, D. Y. Noh, T. Matsunaga, H. Okino, and T. Yamamoto, Ferroelectrics **328**, 69 (2005).
[13]S. Yokoyama, Sa. Okamoto, Sh. Okamoto, H. Funakubo, H. Matsuda, T. Iijima, K. Saito, H. Okino, and T. Yamamoto, J. Appl. Phys. **98**, 086112 (2005).
[14]S. Yokoyama, Sa. Okamoto, H. Funakubo, T. Iijima, K. Saito, H. Okino, T. Yamamoto, K. Nishida, T. Katoda, and J. Sakai, J. Appl. Phys. **100**, 054110 (2006).
[15]F. Kurokawa, Y. Tsujiura, H. Hida, and I. Kanno, Jpn. J. Appl. Phys., Part 1 **53**, 09PA06 (2014).
[16]See supplementary material at http://dx.doi.org/10.1063/1.4944774 for X-ray diffraction data and visual explanation of permittivity measurements.
[17]Y. S. Kim, J. S. Choi, J. Kim, S. J. Moon, B. H. Park, J. Yu, J.-H. Kwon, M. Kim, J.-S. Chung, T. W. Noh, and J.-G. Yoon, Appl. Phys. Lett. **97**, 242907 (2010).
[18]R. A. Rao, Q. Gan, C. B. Eom, R. J. Cava, Y. Suzuki, J. J. Krajewski, S. C. Gausepohl, and M. Lee, Appl. Phys. Lett. **70**, 3035 (1997).
[19]S. D. Bu, M. K. Lee, C. B. Eom, W. Tian, X. Q. Pan, S. K. Streiffer, and J. J. Krajewski, Appl. Phys. Lett. **79**, 3482 (2001).
[20]D. Schlom, L. Chen, C. Eom, K. Rabe, S. Streiffer, and J. Triscone, Annu. Rev. Mater. Res. **37**, 589 (2007).
[21]R. Keech, S. Shetty, M. A. Kuroda, X. H. Liu, G. J. Martyna, D. M. Newns, and S. Trolier-McKinstry, J. Appl. Phys. **115**, 234106 (2014).
[22]V. Nagarajan, S. P. Alpay, C. S. Ganpule, B. K. Nagaraj, S. Aggarwal, E. D. Williams, A. L. Roytburd, and R. Ramesh, Appl. Phys. Lett. **77**, 438 (2000).
[23]M. E. Drougard and R. Landauer, J. Appl. Phys. **30**, 1663 (1959).
[24]C. Zhou and D. M. Newns, Superlattices Microstruct. **23**, 539 (1998).
[25]D. Tenne, A. Clark, A. James, K. Chen, and X. Xi, Appl. Phys. Lett. **79**, 3836 (2001).
[26]U. Aschauer, R. Pfenninger, S. M. Selbach, T. Grande, and N. A. Spaldin, Phys. Rev. B **88**, 054111 (2013).
[27]I. B. Misirlioglu, M. B. Okatan, and S. P. Alpay, J. Appl. Phys. **108**, 034105 (2010).
[28]C. K. Wong and F. G. Shin, Appl. Phys. Lett. **86**, 042901 (2005).
[29]X. J. Zheng, W. Yin, T. Zhang, Q. Chen, M. H. Tang, and J. Sun, Phys. Status Solidi RRL **3**, 251 (2009).
[30]J. Narvaez and G. Catalan, Appl. Phys. Lett. **104**, 162903 (2014).
[31]J. P. Maria, J. F. Shepard, S. Trolier-McKinstry, T. R. Watkins, and A. E. Payzant, Int. J. Appl. Ceram. Technol. **2**, 51 (2005).